❑   597

Dynamics and Control of a Stop Rotor Unmanned Aerial Vehicle

Alvaro Vargas-Clara, Sangram Redkar
Department of Engineering, Arizona State University

Article Info	ABSTRACT
	The objective of this work was to develop a variety of control systems for a Stop-Rotor Unmanned Aerial Vehicle (UAV) in hover flight. The Stop-Rotor UAV has capabilities of Vertical Take-off and Landing (VTOL) like a helicopter and can convert from a helicopter mode to an airplane mode in mid-flight. Thus, this UAV can hover as a helicopter and achieve high mission range of an airplane. The stop-rotor concept implies that in mid-flight the thrust generating helicopter rotor stops and rotates the blades into airplane wings. The thrust in airplane mode is then provided by a pusher propeller. The aircraft configuration presents unique challenges in flight dynamics, modeling and control. In this paper a mathematical model is derived, and then the model is simulated with non-zero initial conditions. Various control systems are then implemented. The control techniques utilized are a linear control, optimal linear control and a nonlinear control with the objective of stabilizing the UAV in hover flight. Settling time and control effort are then compared across the different control systems.

Corresponding Author:

Sangram Redkar,
Department of Engineering,
Arizona State University,
7171 E Sonoran Arroyo Mall, Peralta Hall 330 T, Mesa, Arizona 85212, US.
Email: sredkar@asu.edu.

1.   INTRODUCTION

There have been countless efforts to develop an aircraft that has the versatility of a helicopter and the endurance, range and speed of an airplane. An aircraft with such capabilities would be considered an ideal aircraft. A promising effort is the concept of a stop-rotor configuration. The stop-rotor concept incorporates the flight characteristics of a helicopter and of an airplane. However, unlike prior attempts such as a tilt-rotor aircraft, the stop-rotors' thrust generating device in both flight modes is uncompromised in terms of performance. The stop-rotor concept is defined by the method in which it converts between the flight- modes, thus the rotor that provides thrust in helicopter mode is stopped in mid-flight and it is then used as a lifting surface in fixed-wing flight.

Currently, there are two types of stop-rotors, one being of radial-flow conversion. In radial stop-rotor design approach the rotor disc is parallel to the air-flow direction during conversion from rotary mode to fixed-wing mode. A radial-flow stop-rotor forces the airfoil to experience approximately 180° change in air-flow direction during conversion between flight modes. This has resulted in very serious compromises and consequences including 50% chord-wise pitching axis placement.. In the development this aircraft, the design induced extreme pitching moment acting on the fuselage which caused it to crash [1]. The way around the design flaw of a radial-flow conversion is to depart from this flow conversion and approach an axial-flow conversion of stop-rotor. The axial-flow conversion stop-rotor design utilizes the process of feathering or pitching propellers. In this stop-rotor flow conversion the air-flow impinging upon the rotor disc plane is perpendicularly, aligned with the rotational axis of the rotor. The principal advantage of an axial flow

conversion compared to the radial flow conversion is that the air-flow impinging on the airfoil does not change direction, so the airfoil can have conventional profiles with aero-elastically stable quarter chord pitch axes.

The focus of this paper will be on the development of a mathematical model and implementation of a hover control system for the Stop-Rotor UAV, which is the first and only stop-rotor concept where the axial flow conversion approach is advanced. The design of this UAV presents unique challenges in flight dynamics, modeling and controls. The objective of this work is to derive and simulate a mathematical model of this unique aircraft in hover flight. In addition, various linear and nonlinear control methods will be implemented to stabilize the aircraft in hover flight under non-zero initial conditions. Comparison of the control methods will be drawn across control effort, and settling time of stabilization. The paper is organized in the following form. First, the Stop-Rotor UAV design is briefly introduced and derivation of the mathematical model is presented in Section 2. The implementation of a linear control, optimal linear control and nonlinear control are presented in Section 3. Simulation and results are presented in section 4. Finally, closing remarks are presented.

2.   PROBLEM STATEMENT

2.1. Stop-Rotor UAV
The unique the design of the Stop-Rotor consists of four major components:
1. Fuselage - accommodates the engine, rotor shaft, clutch and any electrical and navigational hardware.
2. Wings/Bottom Rotor - are of a conventional NACA 0012 airfoil. In helicopter mode the wings are feathered and act as a rotor to counter-act the torque from the tail rotor, while in airplane mode they act like conventional fixed-wings.
3. Tail Rotor - also comprises of a NACA 0012 airfoil. In helicopter the tail rotor is the sole thrust generating mechanism and is the only powered rotor. In an airplane mode the clutch disengages power to the tail rotor and the tail rotor is then feathered and assumes the role of a tail in a conventional fixed-wing aircraft.
4. Push propeller - its sole purpose is to provide thrust in airplane mode. The push propeller is optimized in pitch, blade area and twist to provide the best performance of speed, range and endurance.
Figure 1 illustrates these components in both rotary and fixed-wing aircraft modes.
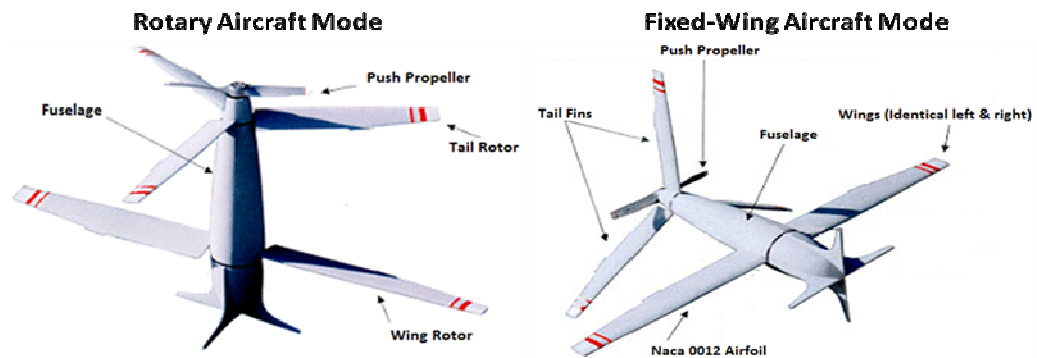

Figure 1. Stop-Rotor UAV in rotary mode (left) and fixed-wing mode (right)

It is important to point out that from the left figure in Figure 1 it can be seen that there is a similarity of this rotary aircraft with a coaxial helicopter. Similar to a coaxial helicopter the Stop-Rotor UAV comprises of two rotors. The tail rotor and the wing rotor, but this is where the similarities end. We will derive a mathematical model of the Stop-Rotor UAV in hover flight. This model will give an insight of the aircraft's stability, controllability and flight dynamics.

2.2. Mathematical Model
The mathematical model primarily focuses on the dynamics of the aircraft in hover flight. The stop-rotor is shown on left figure of Figure 2 along with the coordinate systems used to derive the equations of motion.
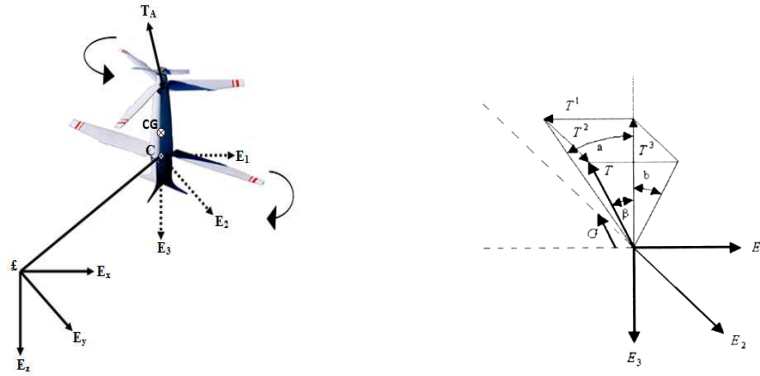
Figure 2. Stop Rotor UAV model representation (left). Thrust vector of *above* (tail) rotor (right) [2]

£ = {E_x, E_y, E_z} is a right hand inertial frame, which is stationary with respect to the earth. Let C = {E_1, E_2, E_3} be a right hand body fixed frame, where CG was the fixed position center of mass of the aircraft. **R**, is an orthogonal rotation matrix. **R** : C→£ denotes the aircraft orientation with respect to £. Where ψ, θ, φ describes yaw, pitch, and roll angles respectively. The rotational matrix that aligns the body fixed frame to the inertial frame was given by:

$$\mathbf{R}\left(\psi,\theta,\phi\right)=\begin{pmatrix} c_\phi c_\psi & s_\phi s_\theta c_\psi - c_\phi s_\psi & c_\phi s_\theta c_\psi + s_\phi s_\psi \\ c_\theta s_\psi & s_\phi s_\theta s_\psi + c_\phi c_\psi & c_\phi s_\theta s_\psi - s_\phi s_\psi \\ -s_\theta & s_\phi c_\theta & c_\phi c_\theta \end{pmatrix}$$

(1)

where $c_\theta = \cos\theta$ and $s_\theta = \sin\theta$. Dynamic model was obtained by with the following assumptions:

- The blades of the two rotors are not hinged, but are directly attached to the hub. As a consequence each rotor blades will always lie in a disk termed rotor disk.
- The tail rotor, denoted by 'A' for *above* rotor, is assumed to rotate in an anti-clockwise direction when viewed from above. The wing rotor, denoted by 'B' for *bottom* rotor, rotates in a clockwise direction.
- It is assumed that the cyclic lateral and longitudinal tilts of the tail rotor disk are measureable and controllable. The tail rotor is the only rotor that has inputs for flapping angles.
- The only air resistances modeled are simple drag forces opposing the rotation of the two rotors.
- Aerodynamic forces generated by the relative wind are not considered
- The interaction of the ground and aircraft is neglected.
- The interaction of the two rotors acting in close proximity will not be considered.

For simplification, the model was split into two major sections. First section covers the translational forces acting on the aircraft. The second section covers the rotational dynamics. A complete model will then be presented that combines these two sections.

2.2.1. Translational Forces

The forces acting on the fuselage of the aircraft were the forces produced by the *above* rotor, *bottom* rotor and lastly due to gravity. Denoted by T_A the thrust generated by the *above* 'A' (Tail) rotor while denoted T_B the thrust generated by the *bottom* 'B' (Wing) rotor. The thrust of the *above* and *bottom* rotor were described as the following:

$$T_A = T_A^1 E_1 + T_A^2 E_2 - T_A^3 E_3$$

(2)

$$T_B = T_B^1 E_1 + T_B^2 E_2 - T_B^3 E_3$$

(3)

Since the *bottom* rotor has no swash plate. The thrust vector of this rotor only has the same direction, i.e. in the direction of the E_3 axis, so Equation **Error! Reference source not found.** was rewritten as:

$$T_B = -T_B^3 E_3$$

(4)

As described in [2], the thrust vector for the *above* rotor was defined as a function of the flapping angle β. The angle represented the tilt of the *above* rotor disk with respect to its initial rotation plane. This

angle consisted of angle *a* (longitudinal flapping) and angle *b* (lateral flapping) in which they were assumed to be measureable and controllable variables. Figure 2 illustrates this correlation (right figure).

Using geometric calculus, the projection of the thrust components of T_A was expressed as:

$$T_A^1 = \frac{-\sin(a)\cdot\cos(b)}{\sqrt{1-\sin^2(a)\cdot\sin^2(b)}}\cdot|T_A| \quad T_A^2 = \frac{\cos(a)\cdot\sin(b)}{\sqrt{1-\sin^2(a)\cdot\sin^2(b)}}\cdot|T_A| \quad T_A^3 = \frac{-\cos(a)\cdot\cos(b)}{\sqrt{1-\sin^2(a)\cdot\sin^2(b)}}\cdot|T_A|$$

(5)

The thrust vector T_A was expressed as

$$T_A = G(a,b)\cdot|T_A|$$

(6)

where,

$$G(a,b) = \frac{1}{\sqrt{1-\sin^2(a)\cdot\sin^2(b)}}\cdot\begin{pmatrix} -\sin(a)\cdot\cos(b) \\ \cos(a)\cdot\sin(b) \\ -\cos(a)\cdot\cos(b) \end{pmatrix}$$

(7)

Lastly, the final force applied to the Stop-Rotor UAV was gravitational force given by:

$$f_g = mgE_z$$

(8)

where, *m* defines the total mass of the aircraft and *g* is the gravity constant. Equation **Error! Reference source not found.** is given in the inertial fixed frame £. So the external total force applied to the aircraft was represented by F:

$$F = T_A + T_B + f_g$$

(9)

$$F = \mathbf{R}G(a,b)\cdot|T_A| - \mathbf{R}T_B^3 E_3 + mgE_z$$

(10)

This is the representation of F on the inertial frame.

2.2.2. Torques and Anti-Torques

Due to the thrusts T_A and T_B the torques were generated. The torques were due to the separation between the center of mass (CG) and the rotor hubs. τ_A and τ_B were denoted as the torques produced by T_A and T_B respectively.

Represented by l_A and l_B were the measured distances from the CG to the hubs of the *above* and *bottom* rotor respectively. So the torques applied to the aircraft were:

$$\tau_A = l_A \times T_A \qquad \tau_B = l_B \times T_B$$

(11)

In addition, the aerodynamic drags acted on the rotors produced pure torques which acted through the rotor hubs. So the anti-torques were defined by:

$$Q_A = |Q_A|E_3 \quad Q_B = -|Q_B|E_3$$

(12)

Lastly, the total torque applied to the aircraft was expressed in the body fixed frame as:

$$\tau = \tau_A + \tau_B + |Q_A|E_3 - |Q_B|E_3$$

(13)

2.2.3. Complete Dynamic Model

By incorporating the total forces and total torques, the following complete dynamic model was obtained in the inertial frame:

$$\dot{\xi} = \mathbf{v}$$

(14)

$$\mathbf{m\dot{v}} = \mathbf{R}G(\mathbf{a,b})\cdot|\mathbf{T_A}| - \mathbf{T_B^3 R E_3} + \mathbf{mgE_z}$$

(15)

$$\mathbf{\dot{R}} = \mathbf{R}\hat{\Omega}$$

(16)

$$\mathbf{I\dot{\Omega}} = -\mathbf{\Omega}\times\mathbf{I\Omega} + \mathbf{\tau_A} + \mathbf{\tau_B} + |\mathbf{Q_A}|\mathbf{E_3} - |\mathbf{Q_B}|\mathbf{E_3}$$

(17)

In the translation movement of the aircraft, let $\dot{\xi}$ (c.f. Equation **Error! Reference source not found.**) defined the velocity, **v**, of the aircraft's CG expressed in its inertial frame £. In Newton's equations of motion $\mathbf{I\dot{\Omega}} = -\Omega\times I\Omega + \tau$ denoted the rotational component of movement in a non-inertial frame, where Ω was the angular velocity in the non-inertial frame; **I** defined the inertia of the aircraft in its CG in respect to the body fixed frame and τ represented the total external torque applied in the body fixed frame.

Also it was important to define that $\Omega \in |R^3$ and

$$\hat{\Omega} = \begin{pmatrix} 0 & -\Omega^3 & \Omega^2 \\ \Omega^3 & 0 & -\Omega^1 \\ -\Omega^2 & \Omega^1 & 0 \end{pmatrix} \tag{18}$$

The mathematical model presented above embodies the dynamics of the aircraft in vector form, but to conduct simulations and analyze the dynamics of the aircraft this model was expanded using Newton-Euler formulation, which is presented in the following section.

2.2.4. The Detailed Mathematical Model

The mathematical model presented in section 2.2.3 was expanded to Newton-Euler form to code and simulate the dynamics of the aircraft in hover flight. The Newton-Euler model was expanded using the same assumptions, and equations previously stated in previous sections as well as using Figure 2 as aircraft model representation. This model expansion was split into two parts, one covering the translation dynamics and the other the rotational dynamics.

For the expanded model, $\mathbf{R}_{exp}$ was defined as:

$$\mathbf{R}_{exp}(\phi, \theta, \psi) = \begin{pmatrix} c_\psi c_\theta & c_\psi s_\theta s_\phi - s_\psi c_\phi & c_\psi s_\theta c_\phi + s_\psi s_\phi \\ s_\psi c_\theta & s_\psi s_\theta s_\phi + c_\psi c_\phi & s_\psi s_\theta c_\phi - s_\phi c_\psi \\ -s_\theta & s_\phi c_\theta & c_\phi c_\theta \end{pmatrix} \tag{19}$$

where $c_\theta = \cos(\theta)$ and $s_\theta = \sin(\theta)$ are used as before.

$\mathbf{R}_{exp}$ is an orthogonal rotation matrix. $\mathbf{R}_{exp}$: C→£ denoted the aircraft orientation with respect to £. The translation dynamics for the expanded Newton-Euler model [3] in the fixed inertial frame £ were:

$$\ddot{E}_X = \frac{1}{m} \cdot \left[\left(c_\psi c_\theta \right) \cdot \left(T_A^1 \right) + \left(s_\psi c_\phi + c_\psi s_\theta s_\phi \right) \cdot \left(T_A^2 \right) + \left(c_\psi s_\theta c_\phi + s_\psi s_\phi \right) \cdot \left(T_A^3 - T_B \right) \right] \tag{20}$$

$$\ddot{E}_Y = \frac{1}{m} \cdot \left[\left(s_\psi c_\theta \right) \cdot \left(T_A^1 \right) + \left(s_\psi s_\theta s_\phi + c_\psi c_\phi \right) \cdot \left(T_A^2 \right) + \left(s_\psi s_\theta c_\phi + s_\phi c_\psi \right) \cdot \left(T_A^3 - T_B \right) \right] \tag{21}$$

$$\ddot{E}_Z = g + \frac{1}{m} \cdot \left[\left(s_\theta \right) \cdot \left(T_A^1 \right) + \left(s_\phi c_\theta \right) \cdot \left(T_A^2 \right) + \left(c_\phi c_\theta \right) \cdot \left(T_A^3 - T_B \right) \right] \tag{22}$$

The expansion of the rotational dynamics in the Newton-Euler's model uncovered the body gyro-effect, rotor gyro-effect, inertial-counter torque and counter torque unbalance. So the rotational dynamics for the expanded model in the fixed inertial frame £ were:

$$I_{xx}\ddot{\phi} = \dot{\theta}\dot{\psi}\left(I_{yy} - I_{zz} \right) - J_B \dot{\theta}\Omega_B + J_A \dot{\theta}\Omega_A + T_A^2 l_A \tag{23}$$

$$I_{yy}\ddot{\theta} = \dot{\phi}\dot{\psi}\left(I_{zz} - I_{xx} \right) + J_B \dot{\phi}\Omega_B - J_A \dot{\phi}\Omega_A + T_A^1 l_A \tag{24}$$

$$I_{zz}\ddot{\psi} = \dot{\phi}\dot{\theta}\left(I_{xx} - I_{yy} \right) + Q_A - Q_B \tag{25}$$

where I_{xx}, I_{yy}, I_{zz} were the moments of inertia of the aircraft about the CG; $J_{A/B}$ were the rotor inertias of the *above* and *bottom* rotor respectively.

To obtain the thrust (T) and drag moment (Q) for the *above* and *bottom* rotor, the momentum theory was used, which is discussed in the following section.

2.2.5. Rotor Aerodynamics

For any airfoil at a certain angle of attack it will produce a lift force and drag force. This is true for a rotor since it basically consists of airfoils pinned at a one end and rotating about the pinned end. In analyzing the two rotors, we obtained the lift and drag forces as in [4]:

$$dL = C_L \cdot \frac{1}{2} \cdot \rho \cdot \left(\Omega \cdot r \right)^2 \cdot c \cdot dr \quad\quad dD = C_D \cdot \frac{1}{2} \cdot \rho \cdot \left(\Omega \cdot r \right)^2 \cdot c \cdot dr \tag{26}$$

where C_L and C_D were the lift and drag coefficients respectively; ρ was the density of air; r was radius location of the blade and c was the chord length of the blade.

Since the objective were to obtain the vertical thrust and horizontal drag moment produced by blades both thrust and drag force have components in the vertical thrust since the blade is pitch at angle $\hat{\phi}$ illustrated in Figure 3.
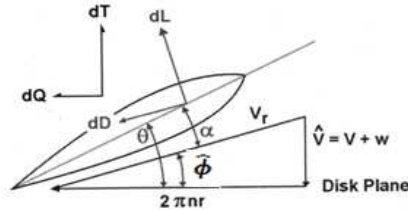
Figure 3. Blade section view

Therefore, thrust force and drag moment were the following:

$$dT = dL \cdot \cos\left(\hat{\phi}\right) - dD \cdot \sin\left(\hat{\phi}\right) \tag{27}$$

$$dQ = \left(dL \cdot \sin\left(\hat{\phi}\right) + dD \cdot \cos\left(\hat{\phi}\right)\right) r \tag{28}$$

Substitute dL and dD into both dT and dQ and integrated with respect to the blade radius we obtained:

$$T_A = \frac{1}{6} C_L \cdot \rho \cdot \Omega_A{}^2 \cdot c_A \cdot R_A{}^3 \cos\left(\hat{\phi}\right) - \frac{1}{6} C_D \cdot \rho \cdot \Omega_A{}^2 \cdot c_A \cdot R_A{}^3 \sin\left(\hat{\phi}\right) \tag{2}$$

Equation (2) is thrust force for a single blade of the *above* rotor. We obtained the total thrust force produced by the *above* rotor by multiplying the equation by the number of blades, *n*, in the rotor.

$$T_A = \left(\frac{1}{6} C_L \cdot \rho \cdot \Omega_A{}^2 \cdot c_A \cdot R_A{}^3 \cos\left(\hat{\phi}\right) - \frac{1}{6} C_D \cdot \rho \cdot \Omega_A{}^2 \cdot c_A \cdot R_A{}^3 \sin\left(\hat{\phi}\right)\right) \cdot n \tag{30}$$

where *n* is 3, or 2 for either the *above* or *bottom* rotor respectively. The drag moment for both *above* and *bottom* rotor was the following:

$$Q = \left(\frac{1}{8} C_L \cdot \rho \cdot \Omega^2 \cdot c \cdot R^4 \sin\left(\hat{\phi}\right) + \frac{1}{8} C_D \cdot \rho \cdot \Omega^2 \cdot c \cdot R^4 \cos\left(\hat{\phi}\right)\right) \cdot n \tag{31}$$

To obtain the value of angular velocity, Ω_A for the *above* rotor the trim condition during hover flight was used:

$$T_A = m g \tag{32}$$

Solve for Ω_A

$$\Omega_A = \sqrt{\frac{mg}{\frac{1}{2} C_L \cdot \rho \cdot c_A \cdot R_A{}^3 \cos\left(\hat{\phi}\right) - \frac{1}{2} C_D \cdot \rho \cdot c_A \cdot R_A{}^3 \sin\left(\hat{\phi}\right)}} \tag{33}$$

To obtain the value of angular velocity, Ω_B for the *bottom* rotor the following condition was used:

$$Q_A - Q_B = J\ddot{\theta} \tag{34}$$

Since in steady hover $\dot{\theta} = 0$, Equation **Error! Reference source not found.** resulted into the following:

$$Q_A = Q_B \tag{35}$$

To solve for the angular velocity, Ω_B for the *bottom* rotor we solved Equation **Error! Reference source not found.** for Ω_B that maded the condition **Error! Reference source not found.** true. So Ω_B was the following:

$$\Omega_B = \sqrt{\frac{3}{2} \cdot \frac{\Omega_A{}^2 \cdot c_A \cdot R_A{}^4}{c_B \cdot R_B{}^4}} \tag{36}$$

This concludes the mathematical model for the Stop–Rotor UAV. The next section will discuss possible control options for controlling the states in the hover flight.

3. CONTROL METHODS

In this section, three control systems were created and implemented to the nonlinear rotational dynamics described in the previous section. The three control systems presented here consist of a linear controller, optimal linear controller and a nonlinear controller. Their main objective was to stabilize the rotational dynamics of the system.

3.1. Linear Controller

First, to create a linear controller for a nonlinear system the system was linearized about an equilibrium solution. The linearized equations of motion were of the form:

$$\ddot{\phi} = \left(\frac{1}{I_{xx}}\right)\left(-J_B\dot{\theta}\Omega_B + J_A\dot{\theta}\Omega_A + T_A^2 l_A\right) \tag{37}$$

$$\ddot{\theta} = \left(\frac{1}{I_{yy}}\right)\left(J_B\dot{\phi}\Omega_B - J_A\dot{\phi}\Omega_A + T_A^1 l_A\right) \tag{38}$$

$$\ddot{\psi} = \left(\frac{1}{I_{zz}}\right)(Q_A - Q_B) \tag{39}$$

To control the rotational dynamics the system command inputs were included in roll, pitch, and yaw to stabilize the dynamics. With addition of the command inputs the linearized state equations took the following form:

$$\ddot{\phi} = \left(\frac{1}{I_{xx}}\right) \cdot (-J_B \cdot \dot{\theta} \cdot \Omega_B + J_A \cdot \dot{\theta} \cdot \Omega_A + T_{act\,Roll}) \tag{40}$$

$$\ddot{\theta} = \left(\frac{1}{I_{yy}}\right) \cdot (J_B \cdot \dot{\phi} \cdot \Omega_B - J_A \cdot \dot{\phi} \cdot \Omega_A + T_{act\,Pitch}) \tag{41}$$

$$\ddot{\psi} = (\frac{1}{I_{zz}}) \cdot (T_{act\,Yaw}) \tag{42}$$

where, $T_{act\,Roll}$, $T_{act\,Pitch}$, and $T_{act\,Yaw}$ were command inputs for roll, pitch, and yaw respectively. The next step for linearization of the system was to convert it to state-space form.

$$\frac{d}{dt}\begin{Bmatrix}\phi\\\dot{\phi}\\\theta\\\dot{\theta}\\\psi\\\dot{\psi}\end{Bmatrix} = \begin{bmatrix}0 & 1 & 0 & 0 & 0 & 0\\0 & 0 & 0 & \dfrac{-J_B\Omega_B + J_A\Omega_A}{Ixx} & 0 & 0\\0 & 0 & 0 & 1 & 0 & 0\\0 & \dfrac{J_B\Omega_B + J_A\Omega_A}{Iyy} & 0 & 0 & 0 & 0\\0 & 0 & 0 & 0 & 0 & 1\\0 & 0 & 0 & 0 & 0 & 0\end{bmatrix}\begin{Bmatrix}\phi\\\dot{\phi}\\\theta\\\dot{\theta}\\\psi\\\dot{\psi}\end{Bmatrix} \tag{3}$$

The system (3) was now linearized. By analyzing the equations in yaw and rate of yaw, we concluded that yaw is independent of roll and pitch, but roll and pitch were dependent on upon each other. The linear controller was of the following form:

$$\dot{x} = A x + B u(t) \tag{4}$$

where, $\dot{x}$ was a state rate, $\mathbf{A}$ was the state matrix, $\mathbf{B}$ was the controller matrix and, $\mathbf{u}$(t)=$\mathbf{Kx}$ in which $\mathbf{K}$ was a matrix of control gains. With the above assumption the controller was of the form $\mathbf{B} \cdot \mathbf{Kx}$ giving the following state control inputs of:

$$\begin{aligned}T_{act_{Roll}} &= K_1\phi + K_2\dot{\phi} + K_3\theta + K_4\dot{\theta}\\T_{act_{Pitch}} &= K_5\phi + K_6\dot{\phi} + K_7\theta + K_8\dot{\theta}\\T_{act_{Yaw}} &= K_9\psi + K_{10}\dot{\psi}\end{aligned} \tag{5}$$

where:

$$\begin{aligned}K_1 &= K1 + K7 & K_2 &= K2 + K8 & K_3 &= K3 + K9 & K_4 &= K4 + K10\\K_5 &= K13 + K19 & K_6 &= K14 + K20 & K_7 &= K15 + K21 & K_8 &= K16 + K22\\K_9 &= K29 + K35 & K_{10} &= K30 + K36\end{aligned} \tag{6}$$

The approach here was to determine the gains in the matrix $\mathbf{K}$ that produced all negative real parts for the eigenvalues for the matrix $[\mathbf{A} - \mathbf{BK}]$. This proved to be rather challenging since the characteristic polynomial was extremely intricate and long. The strategy was to obtain the characteristic polynomial to be of the form:

$$a_0\lambda^6 + a_1\lambda^5 + a_2\lambda^4 + a_3\lambda^3 + a_4\lambda^2 + a_5\lambda + a_6 \tag{7}$$

Then, using the stability criteria of Routh-Hurwitz and Lienard-Chipart to obtain conditions for the gains that would yield the eigenvalues of matrix $[\mathbf{A} - \mathbf{BK}]$ with negative real parts. One of the possible solutions was to use rate and state feedback type controller with

$$K_3 = 0, K_4 = 0, K_5 = 0, K_6 = 0 \tag{8}$$

With the above assumption the state control inputs in Equation (5) was reduced to the following:

$$T_{act_{Roll}} = K_1\phi + K_2\dot{\phi}$$
$$T_{act_{Pitch}} = K_7\theta + K_8\dot{\theta} \qquad (9)$$
$$T_{act_{Yaw}} = K_9\psi + K_{10}\dot{\psi}$$

where K_1, K_2, K_7, K_8, K_9, and K_{10} are all gains that can be selected. This allows for the command input of roll, pitch and yaw for stabilization of those states. Through a number of trials the chosen values of the gains were determined. These gain values were chosen to be:

$$K_1 = -175 \quad K_2 = -58 \quad K_7 = -175 \quad K_8 = -58$$
$$K_9 = -1 \qquad K_{10} = -2 \qquad (10)$$

These gains resulted in the following closed loop eigenvalues for the system

$$\lambda = \{-55.42 + 26.34i \quad -55.42 - 26.34i \quad -2.58 + 1.22i \quad -2.58 - 1.22i \quad -1 \quad -1\}^T \quad (11)$$

Upon selecting the non-optimal gains by trials for the linear controller, the controller was implemented into the nonlinear rotational dynamics. In doing this, it was possible to check whether the linear controller was effective at stabilizing the nonlinear rotational dynamics. So the nonlinear rotational dynamics incorporating the linear controller was the following:

$$\ddot{\phi} = \left(\frac{1}{Ixx}\right) \cdot \left(\dot{\theta}\dot{\psi}\left(I_{yy} - I_{zz}\right) - J_B\dot{\theta}\Omega_B + J_A\dot{\theta}\Omega_A + K1\cdot\phi + K2\cdot\dot{\phi}\right)$$

$$\ddot{\theta} = \left(\frac{1}{Iyy}\right) \cdot \left(\dot{\phi}\dot{\psi}\left(I_{zz} - I_{xx}\right) + J_B\dot{\phi}\Omega_B - J_A\dot{\phi}\Omega_A + K3\cdot\theta + K4\cdot\dot{\theta}\right) \qquad (12)$$

$$\ddot{\psi} = \left(\frac{1}{Izz}\right) \cdot \left(\dot{\phi}\dot{\theta}\left(I_{xx} - I_{yy}\right) + K5\cdot\psi + K6\cdot\dot{\psi}\right)$$

3.2. Optimal Linear Controller

An optimal linear controller was designed comprising of the linear controller described by Equation (5). To design an optimal linear controller it entitled selecting the gains that minimized the cost function:

$$J\left(\mathbf{x}(t),\mathbf{u}(t)\right) = \frac{1}{2}\cdot\mathbf{x}^T\left(tf\right)\cdot\mathbf{H}\cdot\mathbf{x}(tf) + \frac{1}{2}\int_0^{tf}\mathbf{x}^T(t)\cdot\mathbf{Q}\cdot\mathbf{x}(t) + \mathbf{R}\cdot\mathbf{u}^2(t)dt \qquad (13)$$

where $\mathbf{H}$, $\mathbf{Q}$ and $\mathbf{R}$ were all positive semi-definite matrices of size 6x6. $\mathbf{H}$ was assumed to be a zero matrix, while $\mathbf{Q}$ and $\mathbf{R}$ were assumed to be identity matrices. Matrix $\mathbf{Q}$ was multiplied by a factor of 100 indicating the weight on the states. The best approach to minimize the cost function was to reduce $\mathbf{u}(t)$ which as previously mention was $\mathbf{u}(t) = \mathbf{K}(t)\mathbf{x}(t)$. One method for finding the optimal feedback gain matrix was utilizing a nonlinear matrix differential equation, known as the Riccati equation.

$$\dot{\mathbf{S}}(t) = -\mathbf{S}(t)\cdot\mathbf{A} - \mathbf{A}^T\cdot\mathbf{S}(t) + \mathbf{Q} + \mathbf{S}(t)\cdot\mathbf{B}\cdot\mathbf{R}^{-1}\cdot\mathbf{B}^T\cdot\mathbf{S}(t) \qquad (14)$$

The Riccati equation has only final conditions and can be solved backward in time using numerical integration. The solution of an optimal control was reduced by finding the matrix $\mathbf{S}(t)$. The optimal gains were therefore given by:

$$\mathbf{K}(t)\mathbf{x}(t) = \mathbf{R}^{-1}\mathbf{B}^T\mathbf{S}(t)\mathbf{x}(t)$$
$$(15)$$

Using MATLAB, a code was written to numerically integrated the Riccati equation using ode45. The results $\mathbf{S}(t)$ were then inputted into Equation (15). The results led to the population of the $\mathbf{K}$ matrix with optimal gains:

$$\mathbf{K} = \begin{bmatrix} 4.97 & 6.31 & 5.03 & -1.33 & 0 & 0 \\ 4.97 & 6.31 & 5.03 & -1.33 & 0 & 0 \\ -5.03 & -1.33 & 4.97 & 8.99 & 0 & 0 \\ -5.03 & -1.33 & 4.97 & 8.99 & 0 & 0 \\ 0 & 0 & 0 & 0 & 7.07 & 7.55 \\ 0 & 0 & 0 & 0 & 7.07 & 7.55 \end{bmatrix} \qquad (16)$$

Consequently the controller was of the form $\mathbf{B}\cdot\mathbf{Kx}$ giving the following state control inputs similar to the ones in Equation (5). Where the gains in (6) now had the following values:

$$K_1 = -9.95 \quad K_2 = -12.61 \quad K_3 = -10.05 \quad K_4 = 2.66 \quad K_5 = 10.05$$
$$K_6 = 2.66 \quad K_7 = -9.95 \quad K_8 = -17.99 \quad K_9 = -14.14 \quad K_{10} = -15.11$$
$$(17)$$

These were the optimal linear gains. The optimal linear controller was then incorporated into the nonlinear rotational dynamics as

$$\ddot{\phi} = \left(\frac{1}{Ixx}\right) \cdot \left(\dot{\theta}\dot{\psi}\left(I_{yy} - I_{zz}\right) - J_B\dot{\theta}\Omega_B + J_A\dot{\theta}\Omega_A + K1\cdot\phi + K2\cdot\dot{\phi} + K3\cdot\theta + K4\cdot\dot{\theta}\right)$$

$$\ddot{\theta} = \left(\frac{1}{Iyy}\right) \cdot \left(\dot{\phi}\dot{\psi}\left(I_{zz} - I_{xx}\right) + J_B\dot{\phi}\Omega_B - J_A\dot{\phi}\Omega_A + K1\cdot\phi + K2\cdot\dot{\phi} + K3\cdot\theta + K4\cdot\dot{\theta}\right) \quad (18)$$

$$\ddot{\psi} = \left(\frac{1}{Izz}\right) \cdot \left(\dot{\phi}\dot{\theta}\left(I_{xx} - I_{yy}\right) + K5\cdot\psi + K6\cdot\dot{\psi}\right)$$

In this form it is clearly evident that the controller inputs for roll and pitch were dependent on each other to stabilize the roll and pitch. It was also evident that yaw is independent of both roll and pitch.

3.3. Nonlinear Controller

It can be noted that the linear control may work on the nonlinear plant but stability cannot be guaranteed. Also as the initial conditions deviate from equilibrium solution the linear control may not work as the nonlinear effects become predominant. In order to achieve 'global' stability a nonlinear control was proposed. The approach here would be to design the nonlinear controller using Lyapunov approach. In specifically the Lyapunov's direct method. This method is widely used in the stability analysis of general dynamical systems. It makes use of a Lyapunov function $V(\mathbf{x},t)$. This scalar function of the state and time may be considered as some form of time dependent generalized energy. The basic idea of the method is to utilize the time rate of energy change in $V(\mathbf{x},t)$ for a given system to judge whether the system is stable or not. The details about Lyapunov's method and stability theorems can be found in the text [5]. For a linear system where constant coefficients are concerned, it is simple to find a Lyapunov function. Consider the linear system

$$\dot{\mathbf{x}}(t) = \tilde{\mathbf{A}}\mathbf{x}(t) \tag{59}$$

where $\mathbf{A}$ is a constant matrix. A quadratic form of $V(\mathbf{x})$ may be assumed as

$$V(\mathbf{x}) = \mathbf{x}^T\mathbf{P}\mathbf{x}$$

where $\mathbf{P}$ is a real, symmetric and positive definite matrix. Then

$$\dot{V}(\mathbf{x}) = \dot{\mathbf{x}}^T\mathbf{P}\mathbf{x} + \mathbf{x}^T\mathbf{P}\dot{\mathbf{x}} = (\tilde{\mathbf{A}}\mathbf{x})^T\mathbf{P}\mathbf{x} + \mathbf{x}^T\mathbf{P}\tilde{\mathbf{A}}\mathbf{x} \tag{60}$$

or

$$\dot{V}(\mathbf{x}) = \mathbf{x}^T(\tilde{\mathbf{A}}^T\mathbf{P} + \mathbf{P}\tilde{\mathbf{A}})\mathbf{x} \tag{61}$$

According to the Lyapunov theorem for autonomous systems, if $\dot{V}(x)$ is negative definite then the null solution is asymptotically stable [6]. Therefore, one can write [5]:

$$\tilde{\mathbf{A}}^T\mathbf{P} + \mathbf{P}\tilde{\mathbf{A}} = -\mathbf{C} \tag{19}$$

where $\mathbf{C}$ is a positive definite matrix. Equation (19) is called the Lyapunov equation. It has been shown by Bertram and Kalma [7], that if $\tilde{\mathbf{A}}$ has eigenvalues with negative real parts (asymptotically stable), then for every given positive definite matrix $\mathbf{C}$, there exists a unique Lyapunov matrix $\mathbf{P}$. In this study, matrix $\mathbf{C}$ is always taken as the identity matrix. The following Lyapunov function was selected that is always positive definite.

$$V = \phi^2 + \theta^2 + \psi^2 + \dot{\phi}^2 + \dot{\theta}^2 + \dot{\psi}^2 \tag{63}$$

where V is Lyapunov function. The derivative of Equation **Error! Reference source not found.** takes the following form:

$$\dot{V} = 2\dot{\phi}\ddot{\phi} + 2\phi\dot{\phi} + 2\dot{\theta}\ddot{\theta} + 2\theta\dot{\theta} + 2\dot{\psi}\ddot{\psi} + 2\psi\dot{\psi} \tag{64}$$

If v is negative definite, then the nonlinear rotational dynamics will be globally asymptotically stable. So the rotational dynamics for $\ddot{\phi}, \ddot{\theta},$ and $\ddot{\psi}$ were substituted into Equation **Error! Reference source not found.** yielding.

$$\dot{V} = \frac{2\dot{\phi}}{I_{xx}}\left[\dot{\theta}\dot{\psi}\left(I_{yy} - I_{zz}\right) - J_B\dot{\theta}\Omega_B + J_A\dot{\theta}\Omega_A + T_{act_{Roll}}\right] + 2\phi\dot{\phi}$$

$$+ \frac{2\dot{\theta}}{I_{yy}}\left[\dot{\phi}\dot{\psi}\left(I_{zz} - I_{xx}\right) + J_B\dot{\phi}\Omega_B - J_A\dot{\phi}\Omega_A + T_{act_{Pitch}}\right] + 2\theta\dot{\theta} \tag{20}$$

$$+ \frac{2\dot{\psi}}{I_{zz}}\left[\dot{\phi}\dot{\theta}\left(I_{xx} - I_{yy}\right) + T_{act_{Yaw}}\right] + 2\psi\dot{\psi}$$

We assumed the nonlinear controller of the form

$$T_{act_{Roll}} = -K_1\dot{\theta}\dot{\psi} - K_2\dot{\theta} - K_3\dot{\phi} - K_4\phi$$
$$T_{act_{Pitch}} = -K_5\dot{\phi}\dot{\psi} - K_6\dot{\phi} - K_7\dot{\theta} - K_8\theta \qquad (21)$$
$$T_{act_{Yaw}} = -K_9\dot{\phi}\dot{\theta} - K_{10}\dot{\psi} - K_{11}\psi$$

where K_1 through K_6 are controllable gains. To determine the appropriate gains that would satisfy condition for Lyapunov stability, assumptions (21) were substituted into Equations(20). After the substitution the gains were obtained as

$$K_1 = I_{yy} - I_{zz} \qquad K_2 = -J_B \cdot \Omega_B + J_A \cdot \Omega_A \qquad K_3 = a \cdot I_{xx}$$
$$K_4 = I_{xx} \qquad K_5 = I_{zz} - I_{xx} \qquad K_6 = J_B \cdot \Omega_B - J_A \cdot \Omega_A \qquad (22)$$
$$K_7 = a \cdot I_{yy}, K_8 = I_{yy} \qquad K_9 = I_{xx} - I_{yy} \qquad K_{10} = a \cdot I_{zz}$$
$$K_{11} = I_{zz}$$

where a is any number that is less than zero. By implementing these gains Equation (20) was reduced to:

$$\dot{V} = -2a\dot{\phi}^2 - 2a\dot{\theta}^2 - 2a\dot{\psi}^2$$
(23)

Thus, Equation (23) will be always negative definite satisfying the condition for Lyapunov stability.

The nonlinear controller along with the gains was implemented into the nonlinear rotational dynamics. Equation (69) illustrates the rotational dynamics with the nonlinear controller.

$$\ddot{\phi} = \left(\frac{1}{Ixx}\right) \cdot \left(\dot{\theta}\dot{\psi}\left(I_{yy} - I_{zz}\right) - J_B\dot{\theta}\Omega_B + J_A\dot{\theta}\Omega_A - \left(I_{yy} - I_{zz}\right)\dot{\theta}\dot{\psi} - \left(-J_B \cdot \Omega_B + J_A \cdot \Omega_A\right)\dot{\theta} - aI_{xx}\dot{\phi} - I_{xx}\phi\right)$$
$$\ddot{\theta} = \left(\frac{1}{Iyy}\right) \cdot \left(\dot{\phi}\dot{\psi}\left(I_{zz} - I_{xx}\right) + J_B\dot{\phi}\Omega_B - J_A\dot{\phi}\Omega_A - \left(I_{zz} - I_{xx}\right)\dot{\phi}\dot{\psi} - \left(J_B \cdot \Omega_B - J_A \cdot \Omega_A\right)\dot{\phi} - aI_{yy}\dot{\theta} - I_{yy}\theta\right)$$
$$\ddot{\psi} = \left(\frac{1}{Izz}\right) \cdot \left(\dot{\phi}\dot{\theta}\left(I_{xx} - I_{yy}\right) - \left(I_{xx} - I_{yy}\right)\dot{\phi}\dot{\theta} - aI_{zz}\dot{\psi} - I_{zz}\psi\right)$$
(24)

4. RESULTS AND ANALYSIS

A code was written in *MATLAB* that simulates the nonlinear rotational dynamics. So first, the nonlinear rotational dynamics were simulated with non-zero initial conditions (IC) and uncontrolled. The rotational dynamics were clearly unstable with non-zero ICs. Figure 4 illustrates the unstable rotational dynamics with non-zero ICs. The next step was to implement the linear controller to the same nonlinear rotational dynamics. So, the linear controller was now introduced to the nonlinear rotational dynamics with identical non-zero ICs. Figure 5 illustrates effect of the linear controller on the nonlinear rotational dynamics.

In Figure 5, it can be noticed that the rotational dynamics were stabilized using linear, nonlinear and an optimal linear control. In case of linear control, the rotational dynamics were locally stabilized. This means that for a given "small" domain of attraction the linear stabilized the nonlinear rotational dynamics. The linear controller also clearly exhibited settling time issues. The settling time was most noticeable in yaw, which approximately took the controller 40 seconds to stabilize it. The settling time could be a cause from using insufficient gains, non-optimal gains or simply the fact that the linear controller was trying to control nonlinear rotational dynamics.
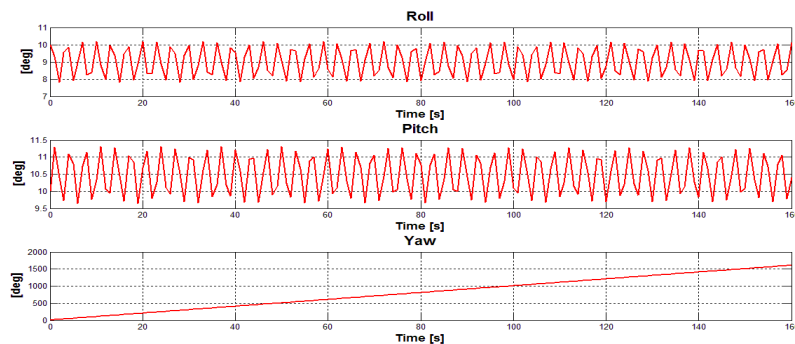
Figure 4. Uncontrolled nonlinear rotational dynamics with non-zero initial condition
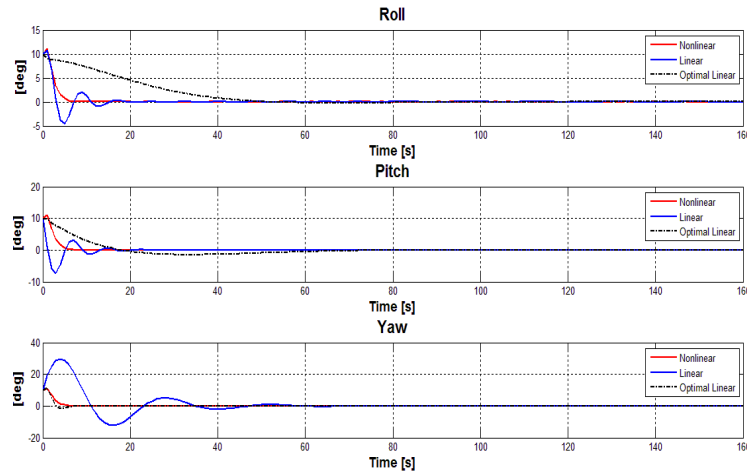

Figure 5. Comparison between nonlinear versus linear versus optimal linear controllers
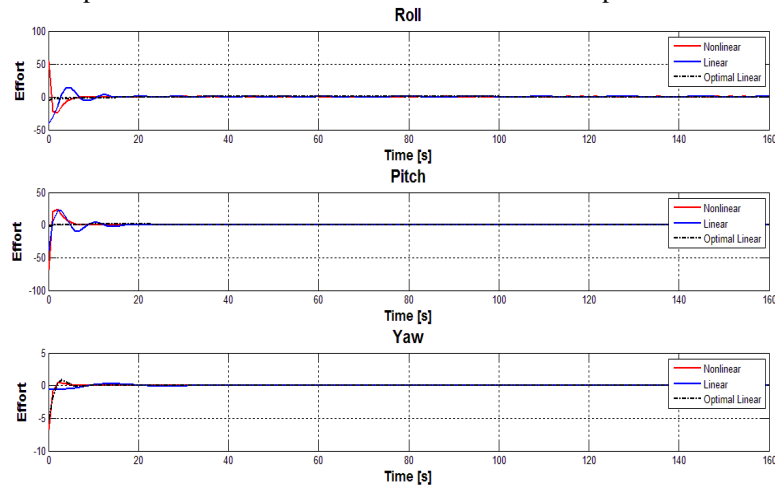

Figure 6. Nonlinear, linear, and optimal linear controller effort

It is important to mention that in similar fashion as the linear controller, the optimal linear control shown in Figure 5, stabilized the rotational dynamics locally. As well, from the Figure 5 it was evident that the optimal controller stabilized yaw faster than roll or pitch, as a result that yaw was independent of roll and pitch. In roll and pitch the issue of settling time was still very present. In the next paragraph the nonlinear controller created was implemented to the same nonlinear rotational dynamics. This allowed us to compare the performance of the linear controller, and optimal linear controller against the nonlinear controller. It was evident that nonlinear controller stabilized the rotational dynamics better than the linear and linear optimal control. It is important to note that the nonlinear controller not only stabilized the rotational dynamics but in addition made the rotational dynamics globally stable. This means the rotational dynamics will always be stable even if large ICs are provided. The nonlinear controller exhibited some settling time. Though, this settling time of the nonlinear controller was much smaller than that of the linear controller or optimal linear controller. Figure 5 illustrates a comparison between the linear controller, optimal linear controller and the nonlinear controller at stabilizing the same rotational dynamics with identical non-zero ICs. Initially the effort for the nonlinear controller at stabilizing the three states (roll, pitch, and yaw) was more than that of the linear and optimal linear controller. As well, the nonlinear controller demonstrated the most effort at the beginning as oppose to the linear and optimal linear controller. The linear controller demonstrated controller effort throughout a larger range of time, while the optimal linear controller demonstrated the least controller effort.

5.   CONCLUSION

In this work, an analysis of dynamics and controllability of a multimode Stop-Rotor UAV was presented. This axial flow stop-rotor is capable of VTOL with ability to transition from helicopter to airplane mode and vice versa in mid-flight.

A mathematical model was developed that captures the stop-rotor dynamics in hover. It is noted that the Stop-Rotor UAV was unstable in hover. So a linear, Linear Quadratic Regulator (LQR) control was designed and implemented to stabilize the hover dynamics. This linear control works when the initial conditions were small and nonlinear effects were not significant. The linear control achieved 'local' stability and may not work for all large disturbances or initial conditions. In order to ensure 'global' stability a Lyapunov approach based nonlinear controller was designed and implemented on the nonlinear plant. The domain of attraction for this nonlinear controller was much higher than the linear controller.

It is anticipated that this work would serve as the foundation to develop a complete autonomous multimode Stop-Rotor UAV. The future work can include simulating the transition equations, design controller for transition dynamics and detailed mathematical analysis that relaxes the assumptions that were used while deriving the equations of motion, to mention a few.

REFERENCES

[1] J. T. McKenna. (2007). "One Step Beyond", *Rotor & Wing*. Retrieved (March 2010) from: http://www.aviationtoday.com/rw/military/medical/One-Step-Beyond_8439.html
[2] P. Castillo, A. E. Dzul, R. Lozano. (2005). Modelling and control of mini-flying machines. 5, 85-94. (ISBN: 1852339578)
[3] S. Bouabdallah. VTOL aircraft dynamic modeling of MAVS. Retrieved (January 2010) from: www.asl.ethz.ch/education/.../2010-L6-Dynamic_Modeling_Rotorcraft.pdf
[4] M. Drier. (2007). Introduction to helicopter and tiltrotor flight simulation, 11, 236-237. (ISBN: 1563478730)
[5] J. S. Bay. (1999). Linear state space systems, 7, 280-285. (ISBN: 0256246394)
[6] W. L. Brogan. (1974). Modern Control Theory. Quantum Publishers, New York.
[7] J. E. Bertram, R. E. Kalman. (1960). Control system and analysis and design via the second method of Liapunov: Parts I and II, Journal of Basic Engineering, Vol 82, pp. 371-400.

BIOGRAPHIES OF AUTHORS

Alvaro Vargas-Clara is currently a Ph.D. student in the Simulation, Modeling and Applied Cognitive Science program. He received his MS degree in Mechanical Engineering Technology from Arizona State University in 2011. He is currently researching bio-inspired control strategies for Unmanned Aerial Vehicles. He is primarly interested in adopting the Brain Emotional Learning model and implementing it for UAV guidance, navigation and control.

Dr. Redkar completed his PhD from Auburn university in 2005. He worked at Archangel system, Auburn from 2005 to 2007. He joined MMET department as an assistant professor in Fall-07. His research interests are nonlinear dynamics, inertial navigation and control.